Identification of the hydantoin alkaloids parazoanthines as novel CXCR4 antagonists by computational and *in vitro* functional characterization

Rosa Maria Vitale[a,#], Stefano Thellung[b,#], Francesco Tinto[a,#], Agnese Solari[b], Monica Gatti[b], Genoveffa Nuzzo[a], Efstathia Ioannou[c], Vassilios Roussis[c], Maria Letizia Ciavatta[a], Emiliano Manzo[a,*], Tullio Florio[b,d,*], Pietro Amodeo[a,*]

[a] Institute of Biomolecular Chemistry, National Research Council (ICB-CNR), Via Campi Flegrei 34, 80078, Pozzuoli, (NA), Italy

[b] Section of Pharmacology, Department of Internal Medicine, University of Genova, 16132 Genova, Italy

[c] Department of Pharmacognosy and Chemistry of Natural Products, Faculty of Pharmacy, School of Health Sciences, National and Kapodistrian University of Athens, Panepistimiopolis Zografou, Athens 15771, Greece.

[d] IRCCS Policlinico San Martino, 16132 Genova, Italy

[#] These authors share co-first authoriship

[*] These authors share co-corresponding authorship

Keywords: hydantoin alkaloids, parazoanthines, natural products, CXCR4 antagonists, molecular docking, pharmacophoric model

Abstract

CXCR4 chemokine receptor represents an attractive pharmacological target due to its key role in cancer metastasis and inflammatory diseases. Starting from our previously-developed pharmacophoric model, we applied a combined computational and experimental approach that led to the identification of the hydantoin alkaloids parazoanthines, isolated from the Mediterranean Sea anemone *Parazoanthus axinellae*, as novel CXCR4 antagonists. Parazoanthine analogues were then synthesized to evaluate the contribution of functional groups to the overall activity. Within the panel of synthesized natural and non-natural parazoanthines, parazoanthine-B was identified as the most potent CXCR4 antagonist with an IC_{50} value of 9.3 nM, even though all the investigated compounds were able to antagonize *in vitro* the down-stream effects of CXC12, albeit with variable potency and efficacy. The results of our study strongly support this class of small molecules as potent CXCR4 antagonists in tumoral pathologies characterized by an hyperexpression of this receptor. Furthermore, their structure-activity relationships allowed the optimization of our pharmacophoric model, useful for large-scale in silico screening.

1. Introduction

Chemokines comprise a family of chemotactic cytokines, classified according to the position of the conserved N-terminal cysteine residues into four main subfamilies: CXC, CC, CX3C and XC [1]. These small proteins exert their homeostatic and/or inflammatory functions by binding and activation of their cognate receptors, the chemokine receptors, belonging to the G-protein coupled receptors (GPCRs) family. CXCR4, the cognate receptor of the C-X-C chemokine CXCL12, is by far the most largely studied chemokine receptor, due to its relevance in many pathologic processes, including HIV infection [2], inflammatory diseases [3–5], cancer [6–9], and WHIM syndrome [10]. In particular, CXCR4 plays a pivotal role in cancer cells survival, proliferation, migration, invasiveness and metastasis, representing a relevant therapeutic target in those diseases characterized by up-regulation of CXCL12/CXCR4 signaling [11]. Currently, the CXCR4 antagonist AMD3100, initially proposed as an anti-HIV agent, is a FDA-approved drug in patients with multiple myeloma and non-Hodgkin's lymphoma who have undergone stem cell transplantation, for its mobilization effect on hematopoietic cells [12]. Starting from AMD3100, other molecules have been developed in an attempt to reduce the size and improve the pharmacokinetic profile, including AMD070 [13], GSK81239 [14], TG-0054 [15], KRH-3955 [16], and HF5073 [17].

In a previous study [18], we developed a minimalistic pharmacophoric model for CXCR4 ligands in which the essential anchoring points on CXCR4 consisted of an aromatic and a basic functional groups, separated by a properly-sized spacer, resulting in an upper limit of 18 Å for the distance between the centers of mass of the two groups. This model led to the identification of phidianidine A (Fig. 1), an alkaloid compound of marine origin, as CXCR4 inhibitor exhibiting low micromolar activity. Natural compounds, representing an invaluable source of novel chemical scaffolds endowed with a high chemical diversity, are very useful in the search of new lead compounds, but their exploitation in drug discovery is often hampered by their limited availability. This is especially true for molecules from marine organisms, and/or when the dimension/complexity of the scaffolds prevents their large-scale synthesis, thus making natural compounds with a low molecular weight and a scaffold easy to synthesize highly desirable. In this view, we included these two latter prerequisites into a new search for naturally-occurring molecules in our ICB collection matching the aforementioned pharmacophoric model. This search identified the parazoanthine (hereafter dubbed as PARA) compound family, hydantoin alkaloids isolated from the Mediterranean Sea anemone *Parazoanthus axinellae* [19,20]. The members of this family of structurally and biologically interesting compounds, currently synthesized at ICB laboratory, share a strongly-basic guanidium moiety separated from a (substituted) p-phenoxy group by a 9-bond spacer including a hydantoin ring (Fig. 1). PARAs differ from each other either in

the substitution pattern of the p-phenoxy group, or in the saturation state of the 5,6 extracyclic bond on the hydantoin ring. According to this latter, PARAs can be classified into saturated (PARA-A,D,F,G,I) and unsaturated (PARA-B,C,E,H,J). As for the aromatic moiety, in this work we only considered the effects of substitution at the oxygen atom of the p-phenoxy group, and its combinations with the 5,6 bond saturation state.

In particular, since parazoanthines A-C had already been synthesized, we started our evaluation checking *in silico* and *in vitro* their ability to act as CXCR4 ligands.

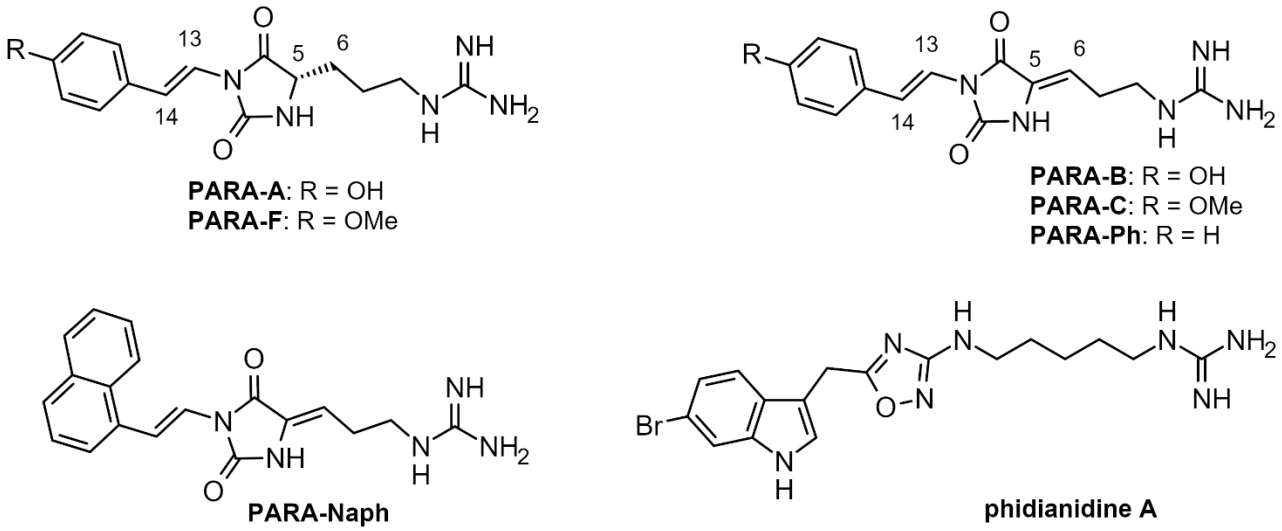

Fig. 1. Structures of PARA-A, PARA-F, PARA-B, PARA-C, PARA-Ph, PARA-Naph and phidianidine A. Relevant numbering is shown on the corresponding atoms.

2. Results and Discussion

2.1. Molecular docking

PARA-A-C differ from each other in the presence of a hydroxy (A-B) or methoxy (C) group on the phenyl ring, and in the number of double bonds in the structure: two ($\Delta_{5,6}$ and $\Delta_{13,14}$) for B-C, respectively, and only one ($\Delta_{13,14}$) for A. They, in turn, differ from phidianidine A, the previously identified CXCR4 antagonist from our ICB collection, in both the aromatic moiety (phenyl vs indole ring) and in the length and nature of the spacer, since they possess a hydantoin group in the place of an oxadiazole ring, and double, in place of single, bond(s) in the carbon chain, as well as in the distance between the two anchoring groups (~14 Å), smaller than that found in phidianidine A. Thus, to rule out possible divergences in the binding modes in comparison to our previous lead phidianidine A, a comprehensive molecular docking study was undertaken. All compounds exhibited a similar arrangement into the binding site as best pose in terms of binding energy, characterized by bidentate ligand-protein H-bonds reinforced by ionic interactions between ligand and Asp97 (helix 2) /Asp187

(loop e2), as well as H-bonds of the hydantoin group with Asp187 side chain and/or carbonyl backbone and the NH backbone atom of Arg188 (loop e2), whereas the ligand aromatic ring is sandwiched between Arg188 and Tyr116 (helix 3) sidechains, with the hydroxy group H-bonded to Thr117 (helix 3) sidechain. This last H-bond does not occur in PARA-C due to the presence of a methoxy group, since Thr117 acts as H-bond acceptor in PARA-A and PARA-B ligands, being its polar hydrogen H-bonded, in turn, to His113 backbone CO. Instead, PARA-C methoxy group forms a H-bond with His203 (helix 5). The occurrence of a double bond in PARA-B does not affect the binding modes since the overall arrangement essentially overlaps that of PARA-A. However, the double bond, by conferring more rigidity to the scaffold, could in principle favourably contribute to the binding by reducing the entropy contribution of the ligand. The representative poses of PARA-B and PARA-C after energy minimization, are shown in Fig. 2A-B. A comparison with phidianidine A shows that PARAs, while exhibiting the same overall arrangement in which the guanidium moiety interacts with the negatively charged residues Asp97 and/or Asp187, and the aromatic pendants are hosted in the same subpocket of the indole moiety of phidianidine A, considerably differ in the favoured arrangements of the central linker. The shorter distance between the aromatic and the basic centers of mass in comparison with phidianidine A, and the H-bonds between the hydantoin ring and the backbone of residues in the e2 loop concur to stabilize a binding mode in which the ligand runs parallel to the e2 loop. Instead, the linker region of phidianidine A allows a greater flexibility of the ligand within the binding site, with the amino-oxadiazole group more distant from the e2 loop and mainly involved in H-bonds with Glu288 on helix 7, which is opposite to the e2 loop in the receptor binding cleft [18]. Furthermore, in order to evaluate the contribution of: a) a H-bond acceptor/donor group on the aromatic pendant, b) the size of the aromatic group, and c) the flexibility of the alkyl chain on ligand activity and/or potency, three derivatives were also considered, featuring phenyl (PARA-Ph) and naphthalene (PARA-Naph) moiety, or a methoxy (correponding to the natural compound PARA-F) [20,21] group on PARA-A. PARA-F, representing the saturated, flexible analogue of PARA-C, completes the set of possible combinations of 5,6 bond saturations state and p-phenoxy oxygen atom substitutions within known unbromurated PARAs. The representative pose of PARA-Naph is shown in Fig. 2C.

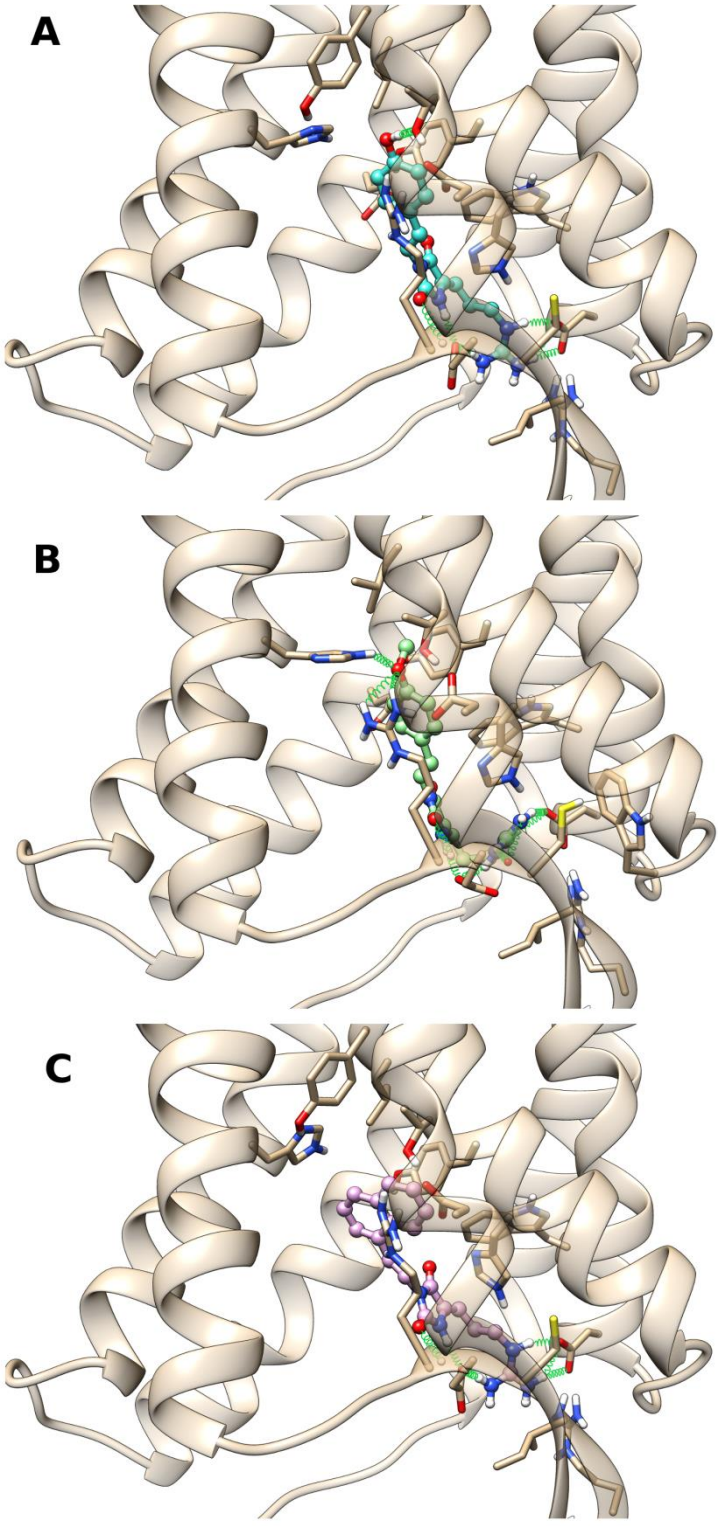

Fig. 2. Ribbon representation of CXCR4 complex with PARA-B (A), PARA-C (B) and PARA-Naph (C). PARA-B, PARA-C and PARA-Naph are shown in ball&stick representation and coloured in cyan, light green and plum, respectively. The residues within 4Å from ligand are shown in stick representation. Nitrogen, oxygen, and sulphur atoms are painted white, blue, red and yellow, respectively.

2.2. Synthesis

2.2.1. Synthesis of PARA-A and O-Me derivative PARA-F

The preparations of the synthetic parazoanthine A (PARA-A) and *O*-methyl derivative (PARA-F) were achieved by a concise biomimetic synthesis based on the coupling reaction of L-arginine methyl ester dihydrochloride with isocyanate derivatives of p-coumaric acid and 4-methoxy-cinnamic acid, respectively. The synthesis of these molecules was performed according to the synthetic procedure of Manzo et al. [22].

2.2.2. Synthesis of PARA-B, PARA-C and PARA-Ph

The natural alkaloids parazoanthines B and C (PARA-B and PARA-C) and the derivative 18-deoxy-parazoanthine B (PARA-Ph) were realized according to the procedure described by Tinto et al. [23].

2.2.3. Synthesis of PARA-Naph

The synthesis of PARA-Naph was inspired by Tinto et al. procedure [23]; we prepared the intermediate α-bromo-1-acetonaphthone by α-bromination of 1-acetonaphthone with bromine in acetic acid (Scheme 1).

The succeeding coupling reaction (Scheme 1) of α-bromo-1-acetonaphthone with the hydantoinic building block (prepared according to [23]), gave the intermediate PARA-Naph-I1; carbonyl reduction of PARA-Naph-I1 with $NaBH_4$ (obtaining intermediate PARA-Naph-I2), and subsequent dehydration with *p*-TsOH in toluene at 110 ° C / 1h led to the intermediate PARA-Naph-I3 free from nitrogen protecting group (BOC) and with E-configuration of 13-14 double bond ($J_{13\text{-}14}$ = 14.8 Hz). Finally, by the guanidination of compound PARA-Naph-I3 using the guanidinating reagent 3,5-dimethyl-1-pyrazolylformaminidium nitrate in basic conditions, we obtained PARA-Naph (Scheme 1). The three last step led to low yield despite the different attempts to improve it by changing reagents amounts (1-4 equivalents) and/or reaction temperature values (from r.t to 110 °C). These yields were the better we obtained.

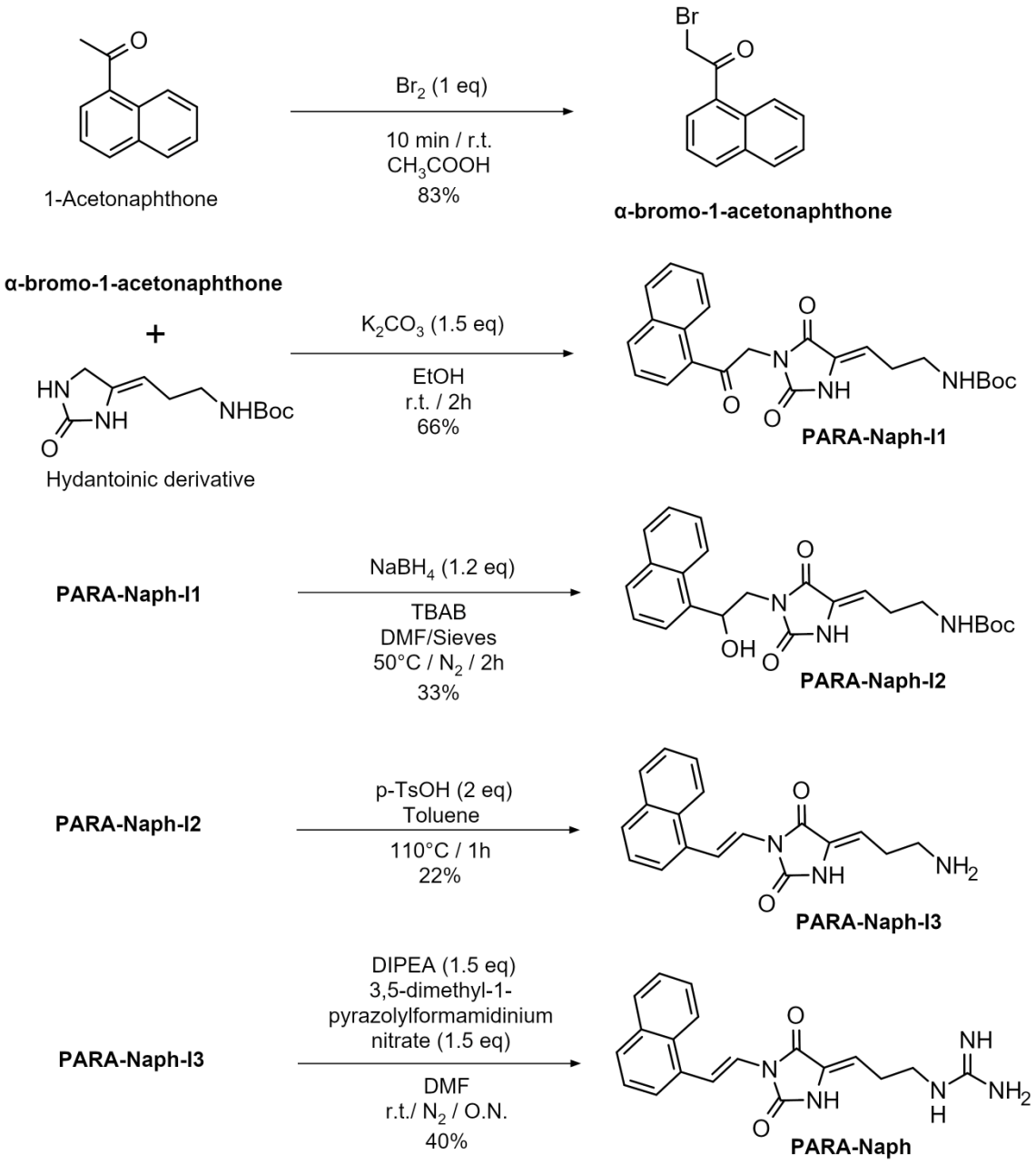

Scheme 1

2.3. Biological assays

GH4C1 cells were used to test the activity of PARA compounds against CXCR4, since this cell line was reported to express CXCR4 but not CXCL12, whose constitutive secretion could interfere with receptor expression [24]. In order to rule out any potential cytotoxic effects of the tested compounds, a cell viability assay was carried out in the absence of CXCL12 stimulation of cell proliferation. Thus, after 48 h of serum deprivation, we treated GH4C1 cells with 1 μM of PARA-A, PARA-Ph, PARA-Naph, PARA-C, PARA-B, PARA-F in FBS-free medium and in the absence of CXCL12; control cells

were treated with the same amount of DMSO, to exclude non-specific effects of the vehicle. After 24 h of incubation, we assayed cells for MTT reduction by mitochondrial enzymes. This test provides a direct index of cell viability, with the obtained values being directly proportional to cells number (Fig. 3). None of the tested molecules induced a significant variation of MTT reduction in GH4C1 cells in comparison with vehicle, indicating that cell viability is not affected by these treatments.

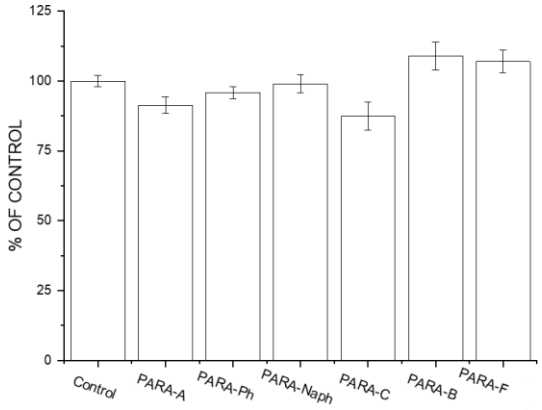

Fig. 3. PARA compounds are not toxic for GH4 C1 cells. GH4C1 cell were treated with all the studied compounds (1μM) and cell viability tested using MTT reduction assay**.**

To address the possibility that PARA molecules may act as CXCR4 antagonists we evaluated their ability to antagonize the mitogenic activity of CXCL12 in GH4C1 cells in concentration-response experiments. For this purpose, we treated FBS-starved GH4C1 cells for 12 h with CXCL12 (25 nM), in the absence or presence of increasing concentrations (10 nM-1 μM) of the molecules under study. Cell proliferation was measured using CyQuant assays that quantify the amount of nucleic acids as a direct index of cells number.

CXCL12 induced a consistent (122 ± 1.4%) and statistically significant ($P > 0.01$) proliferation of GH4C1 cells, as compared to vehicle-treated cells. All tested PARA compounds abolished this effect in a dose-dependent manner, although with different potency (Fig. 4). PARA-B was the most potent CXCR4 antagonist displaying an IC_{50} value of 9.3 nM, followed by PARA-A (18.7 nM), PARA-Naph (70.7 nM), PARA-Ph (116 nM), and PARA-F (269 nM). It was not possible to calculate the IC_{50} value for PARA-C, since the compound showed a biphasic curve, with a strong inhibition at low concentrations (10-50 nM) and a loss of efficacy at high concentrations. As far as efficacy is concerned, all compounds were able to completely abolish CXCL12 proliferative effects, with the exception of PARA-Ph that, even at the highest concentration tested (1 μM), was not able to bring proliferation back to the control level. Moreover, 1 μM PARA-F caused a reduction of GH4C1 DNA content below control levels, as did PARA-C at low concentrations (10-50 nM), raising the possibility of an inverse

agonist activity of these compounds.

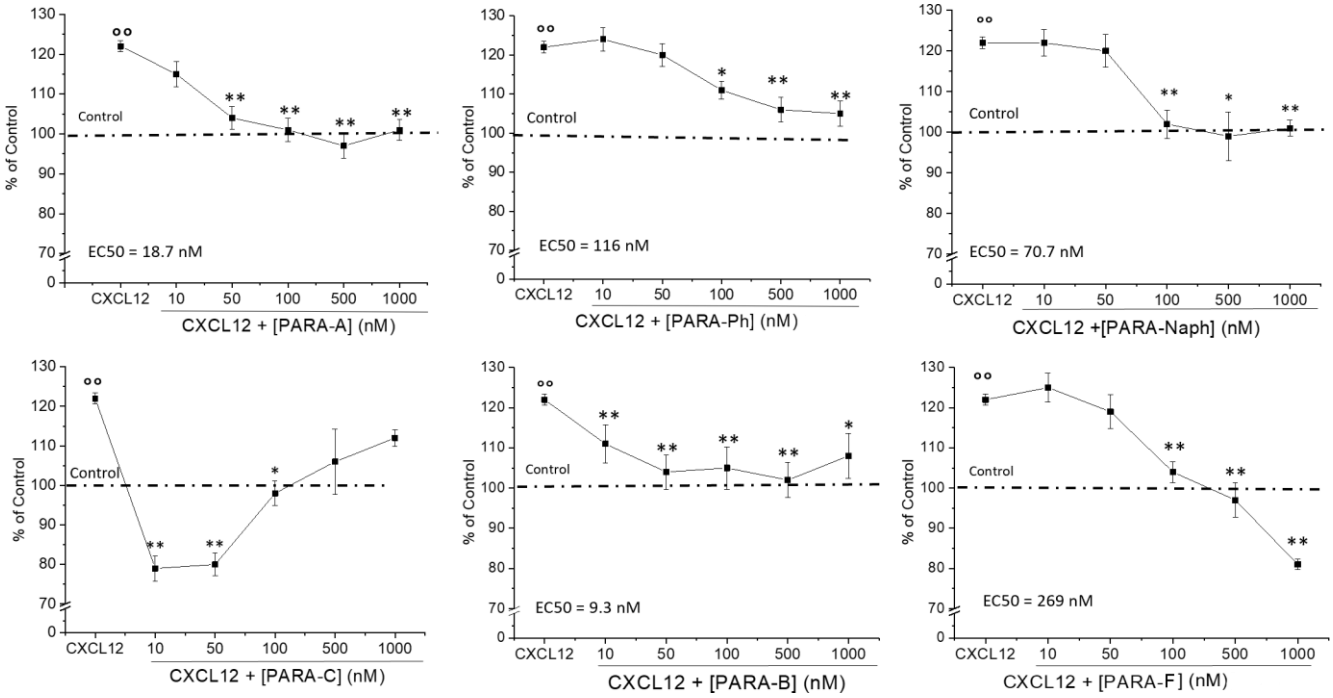

Fig. 4 PARA compounds inhibit GH4C1 proliferation induced by CXCL12. Cells, treated with CXCL12, increased proliferative activity by 22%, an effect concentration-dependently inhibited by all the tested compounds, although with different potency and efficacy. Each panel represent the concentration-response curve (10-1000 nM) of the PARAs on CXCL12 (25 nM)-induced cell proliferation. EC_{50} values are reported within the respective graphs. °° = $p < 0.01$ vs. control values; * and ** = $p > 0.05$ and 0.01 vs. CXCL12.

Linear concentration-dependent activities of PARA-A, PARA-Naph, PARA-Ph, and PARA-B were also demonstrated by measuring the modulation of DNA neosynthesis induced by CXCL12 in GH4C1 cells (Suppl. Fig. 1). By using BrDU incorporation assays we observed that CXCL12-induced GH4C1 cell proliferation was antagonized by these PARA compounds, with similar efficacies to those observed using the CYQuant assay. These results indicate that all tested compounds are able to affect CXCR4 activation concering CXCL12 proliferation signaling, which represents one of the main pathways involved in tumor development, including pituitary adenomas [25,26].

One of the main functions of CXCR4 in normal and tumor cells is the activation of intracellular pathways related to cell motility. To further investigate the efficacy of PARA compounds as CXCR4 antagonists, we evaluated their ability in antagonizing CXCL12-induced GH4C1 cell migration. To this end, we measured the number of cells that permeate through a porous membrane under CXCL12 driving chemotactic force. In our experimental protocol, fluorescence dye-stained GH4C1 cells were seeded into transwell upper chambers, while CXCL12 was added into the lower chambers; the number of chemoattracted cells through the transwell membrane was quantified by counting cells under epifluorescence microscopy after 6 h of migration. Cells were treated with PARA compounds before

their staining and plating in transwell upper chambers (Fig. 5). Vehicle-treated cells displayed a significant sensitivity to CXCL12-dependent migration, as the number of migrating cells increased by 44% in comparison to untreated cells (Fig. 5A). CXCR4 blockade by all PARA molecules, used at 1 μM, significantly reduced the number of migrating cells. Among the tested compounds, PARA-A and PARA-Ph showed lower efficacy, reaching a reduction of CXCL12-induced migration of about 30%, while the remaining showed a greater effect causing about 50% of inhibition (Fig. 5C).

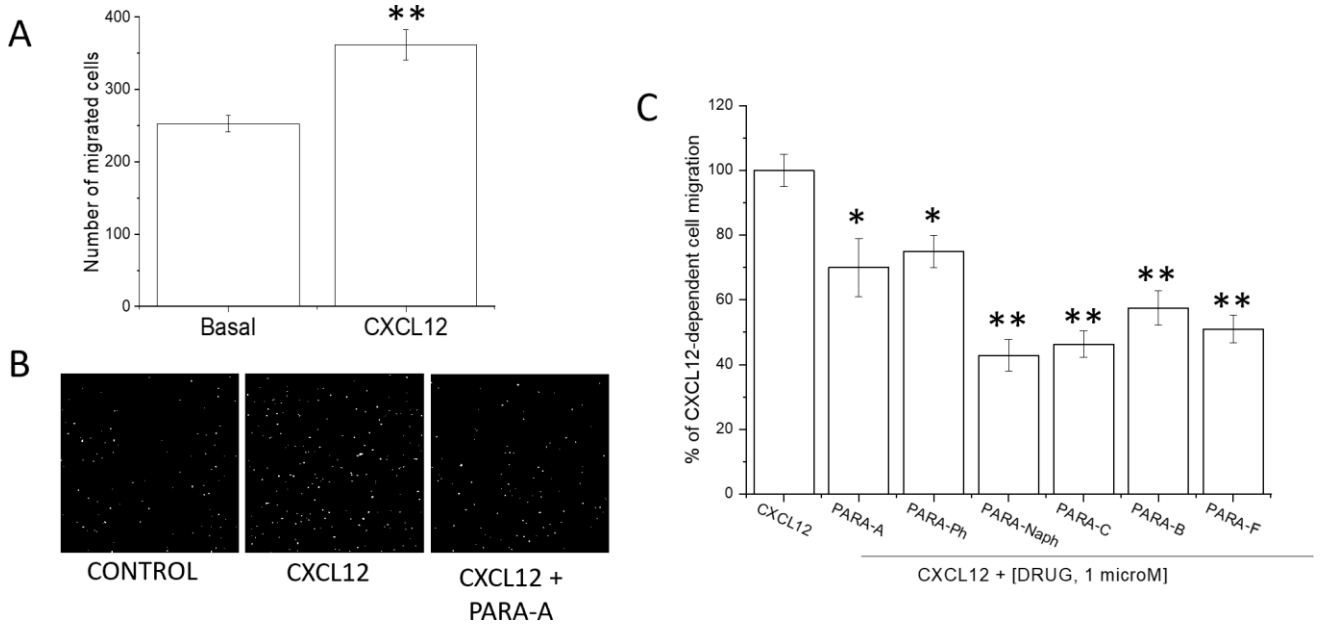

Fig. 5 Effect of PARA compounds on CXCL12-dependent GH4C1 cell migration. A) Cell migration was evaluated using a trans-well approach in which CXCL12 was added to the lower chamber as chemoattractor. Cell migration was monitored taking advantage of the vital Vybrant™ CFDA SE fluorescent dye labelling of GH4C1 cells and measuring fluorescence on the lower side of the trans-well (B) using a fluorescence microscope and the ImageJ software (C). CXCL12 increased GH4C1 cell migration by 44% (A), an effect that was abolished by all the PARA compounds (B, C). * and ** = $p > 0.05$ and 0.01 vs. CXCL12.

ERK1/2 activation is one of the main intracellular signals by which CXCR4 transduces intracellularly external cues [27]. Thus, to confirm the specificity of the observed biological effects we checked whether the tested compounds were able to interfere with CXCL12-dependent phosphorylation/activation of ERK1/2 MAP kinase in GHC1 cells. In particular, we evaluated by immunoblotting ERK1/2 phosphorylation levels after 15 min of treatment with CXCL12 (25 nM), while PARA compounds (50 nM) were added to the cells 30 min before CXCL12 (Fig. 6A). CXCL12 increased ERK1/2 activation by two-fold in respect to basal values, a response that was higher than that elicited by FBS, used as positive control (+113% vs. +61% over basal value, Fig. 6B). Cell pretreatment with all PARA compounds reduced ERK1/2 phosphorylation induced by CXCL12. Among highly statistically significant results ($P < 0.01$ vs. CXCL12 treatment), PARA-B and PARA-C

induced stronger effects, while PARA-Naph elicited a moderate response. The other compounds produced lower effects, with still statistically significant results, although reaching a lower significance ($P<0.05$) (Fig. 6B).

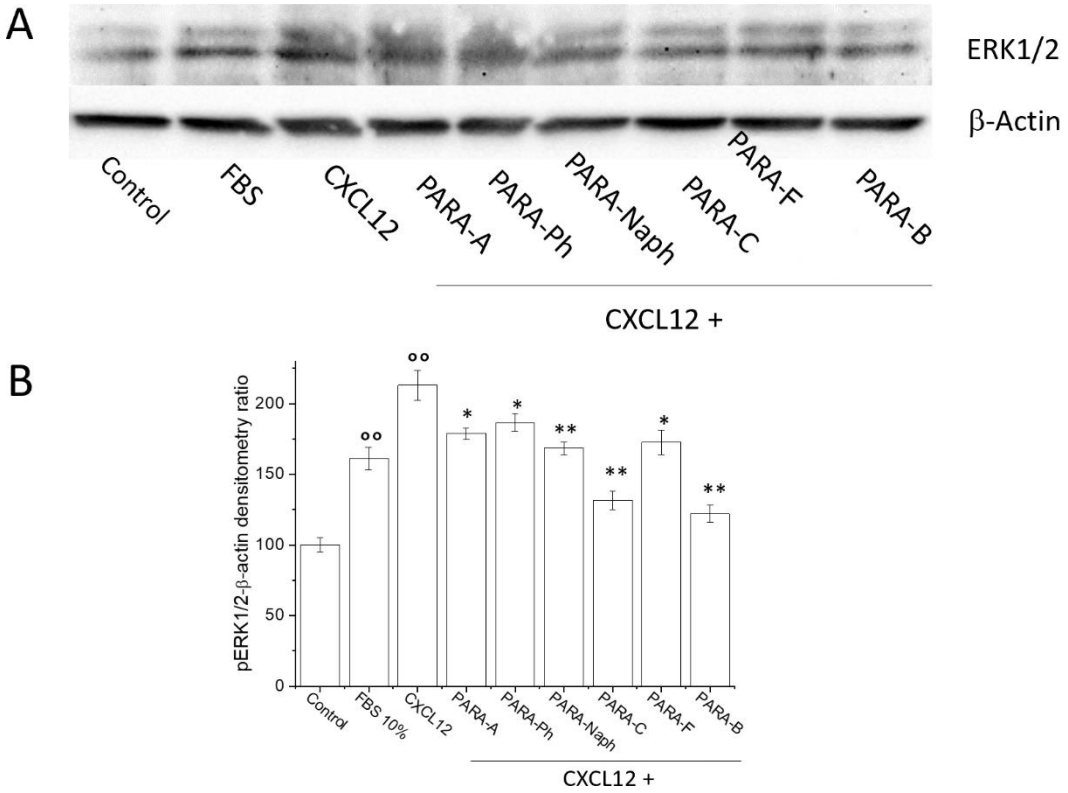

Fig. 6. Effect of PARA s on ERK1/2 activation. ERK1/2 activity in GH4C1 cells evaluated in Western blot using phopsho-specific antibody (A) and quantification by densitometric analysis (B). CXCL12-induced increase of ERK1/2 phosphorylation was significantly reduced by all the PARA compounds tested. °° = $p < 0.01$ vs. control values; * and ** = $p < 0.05$ and 0.01 vs. CXCL12.

Finally, we decided to down-regulate CXCR4 expression in GH4C1 cells to demonstrate that the tested PARA compounds act through an antagonistic activity at this chemokine receptor. We used CRISPR-CAS9) approach to interfere with CXCR4 expression. From gene interference, we selected several clones, 9 of which were expanded and tested for CXCX4 mRNA content by RT-PCR, in comparison to GH4C1 cells (Suppl Fig. 2A). From this screening, we chose the clone A11 that showed the most significant reduction in CXCR4 mRNA (named GH4A11). CXCR4 down-regulation was then confirmed by immunoblotting analysis (Suppl Fig. 2B). Comparing growth ability of GH4A11 and parental GH4C1 cells, using the MTT reduction assay, we did not observe differences in the proliferation rate (data not shown), thus we used this cell line to test the proliferative and migratory activities induced by CXCL12 (25 nM) and the reversal by the PARA compounds (50 nM-1 μM). GH4A11 proliferation rate, evaluated using CyQuant assay, was neither increased by CXCL12 nor reduced in the presence of the PARA compounds, which did not also affect basal growth in the absence

of CXCL12 (Fig. 7). The only significant difference was a slight paradoxical increase of proliferation induced by PARA-B in the presence of CXCL12 ($P<0.05$).

Similar results were also obtained evaluating GH4A11 cell migration, which was neither increased by treatment with CXCL12 nor reduced by all PARA compounds in the presence or absence of CXCL12 (Fig. 8). These results clearly confirmed that the all tested compounds act via CXCR4 antagonism to revert CXCL12 induction of GH4C1 proliferation and migration.

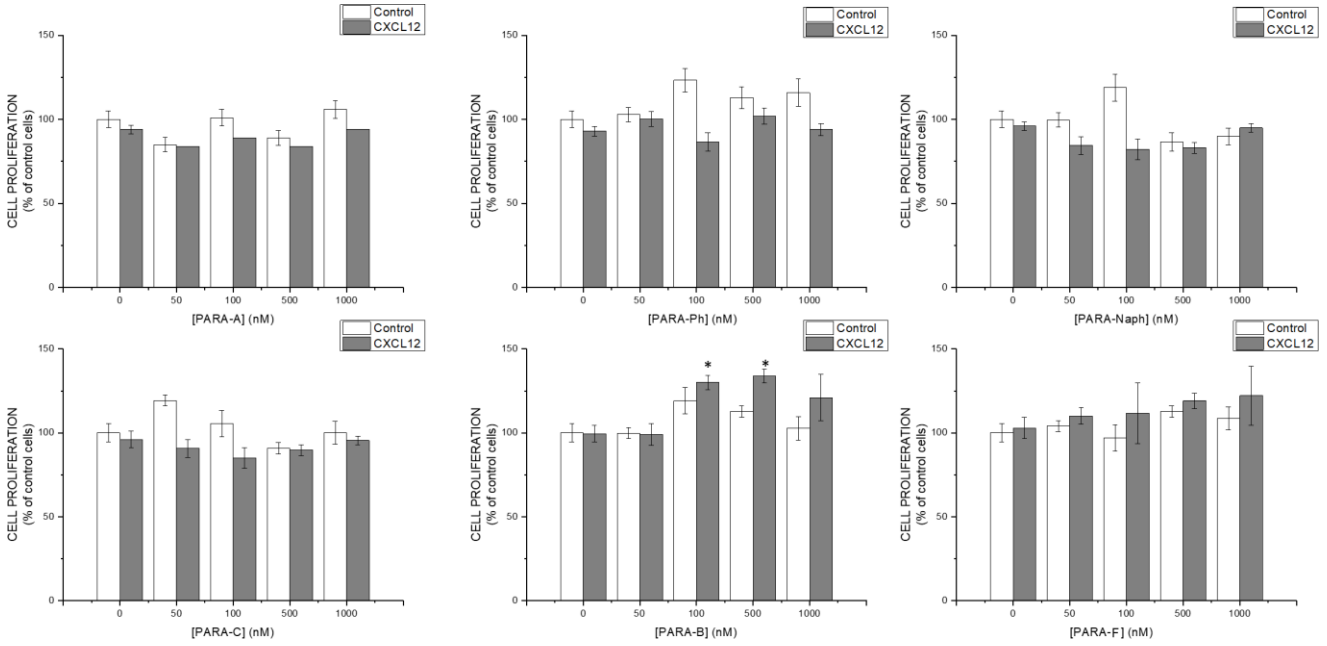

Fig. 7. PARA compounds were unable to modulate GH4A11 cell proliferation, measured by CyQuant evaluation of DNA content, in both basal conditions and in the presence of CXCL12.

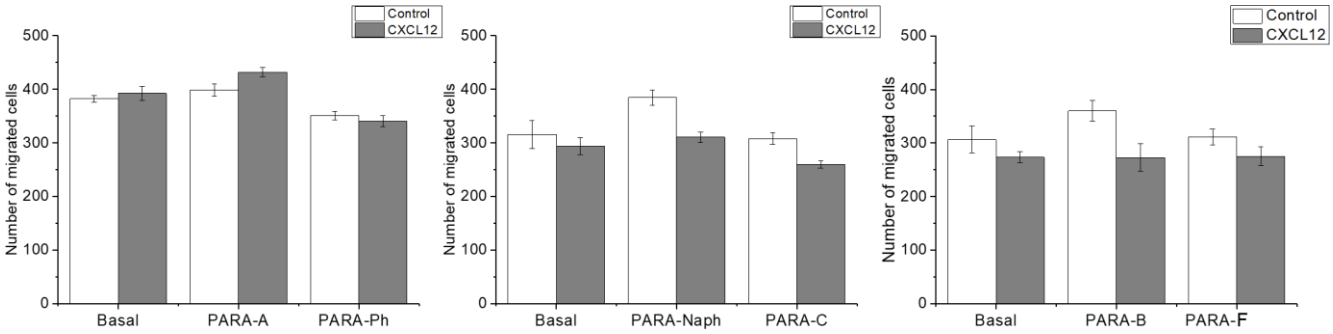

Fig. 8. Lack of PARA compound effects on cell migration in presence of CXCR4 downregulation. In trans well experiments GH4A11 cells showed no responses to both stimulatory effect of CXCL12 and the inhibitory activity of PARA compounds.

2.4. Structure-activity relationships and pharmacophoric model optimization

The activity of PARA compounds as CXCR4 antagonists has been evaluated looking at their ability to counteract the effects of CXCL12/CXCR4 signalling on proliferation, migration and phosphorylation/activation of ERK1/2 MAP kinase (pERK). In all assays, PARA-B was identified as

the most active and potent compound, highlighting the significance of both the double bond on the alkyl spacer and the occurrence of the hydroxy group on the phenyl moiety. In fact, both PARA-A and PARA-Ph were less active than PARA-B, with a more dramatic effect for PARA-Ph. The bulkier naphthalene group performed better than the phenyl substituent on proliferation and migration, but not at pERK assay, suggestive of a biased antagonism effect induced by this substituent, a behaviour already observed by other CXCR4 ligands [28]. The methylation of the hydroxy group is well tolerated in the migration and pERK assays, even increasing the activity of PARA-F in comparison to PARA-A in the migration assay. Instead, in the proliferation assay the methoxy group induces inverse agonism. However, the biphasic curve observed for PARA-C is suggestive of off-target effects at higher concentrations that balance the CXCR4-mediated antiproliferative activity. The comparison between the phidianidine A and parazoanthines B-C scaffolds and the greater potency as CXCR4 antagonists of the latter, suggest that a shorter distance (~14 Å instead of 18 Å) between the guanidine group and the aromatic moiety improves the activity. It is reasonable to speculate that the shorter linker, as well as the two double bonds on the alkyl chain, reduce the flexibility of the ligands, causing in turn a reduction of the unfavourable entropy contribution upon binding. The occurrence of a bulky aromatic group such as the indole group in the phidianidine A or naphthalene in PARA-Naph, is not mandatory for the antagonist activity, but the phenyl group has to compensate the reduced size featuring an hydroxy or methoxy group to engage H-bonds with the polar residues lying in the subpocket hosting the aromatic moiety. Furthermore, in both phidianidine A and parazoanthines, the alkyl linker features a five-membered ring able to form H-bonds with the receptor. Thus, the previous minimalistic pharmacophoric model can be refined as shown in Fig. 9.

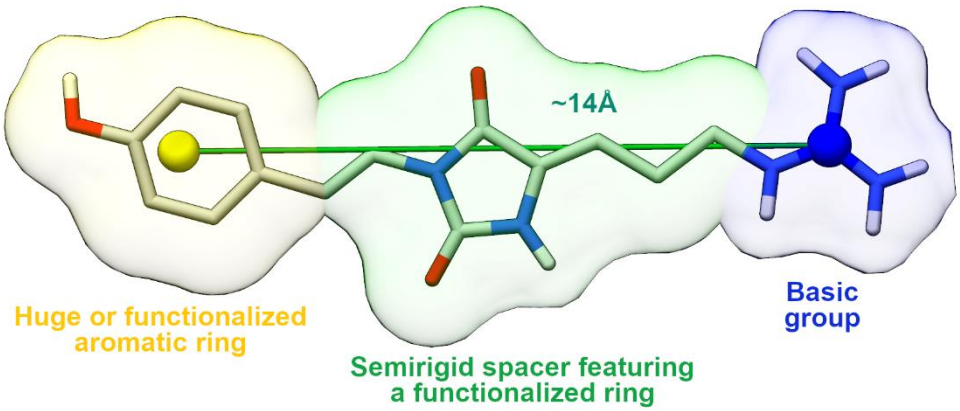

Fig. 9. Optimized pharmacophoric model

3. Conclusions

In conclusion, through a combined computational and experimental approach, we identified parazoanthines as potent CXCR4 antagonists. The validation of the *in silico* results was obtained by assessing the ability of PARA derivatives to antagonize CXCL12-dependent proliferation, migration and phosphorylation/activation of ERK1/2 MAP kinase in rat pituitary adenoma cell line GHC1 cells. All tested compounds were able to antagonize the down-stream effects of CXC12, albeit with variable potency and efficacy, in the low nanomolar-micromolar range. Moreover, these results allowed the development of a more stringent pharmacophoric model, useful for large-scale in silico screening, and candidate PARA derivatives as potentially useful therapeutics tools to negatively modulate the CXCL12/CXCR4 axis in tumoral pathologies characterized by a hyperexpression of this receptor.

4. Experimental part

4.1 Computational Methods

Docking studies were performed with AutoDock 4.2[29]. Both the crystallographic structure of CXCR4 (PDB entry: 3OE0) and the investigated ligands were processed with AutoDock Tools (ADT) package to merge non-polar hydrogens, calculate Gasteiger charges and desolvation parameters, and select all rotatable ligand bonds as flexible. Grids for docking evaluation with a spacing of 0.375 Å and 70x70x50 points, centered in the ligand binding pocket, were generated using the program AutoGrid 4.2 included in Autodock 4.2 distribution. Lamarckian Genetic Algorithm (LGA) was adopted to perform 100 docking runs with the following parameters: 100 individuals in a population with a maximum of 15 million energy evaluations and a maximum of 37000 generations, followed by 300 iterations of Solis and Wets local search. PARA-CXCR4 complexes were selected on the basis of binding energy and cluster population. The x-ray structure was cleaned of the fusion protein at the intracellular loop 3 (IL3) and completed in its not-resolved loop regions using MODELLER program version 9.15[30] and the resulting complexes, after addition of all hydrogen atoms, underwent energy minimization with SANDER module of Amber16 package[31] using the ff14SB version of AMBER force field for the protein and GAFF for the ligand. Ligand atomic charges were obtained with the RESP methodology[32], according to the prescription for molecule parametrization in the GAFF force field. This latter requires an *ab initio* full geometry optimization at the Hartree-Fock level using the STO-3G basis set, followed by a single-point energy calculations on the optimized molecule at the RHF/6-31G* level. *Ab initio* calculations were performed with GAMESS program[33].

4.2. Synthesis (synthetic procedures for PARA-Naph)

NMR spectra of the synthetic compounds were recorded on a Bruker Avance-400 (400.13 MHz) in $CDCl_3$ and CD_3OD (δ values are referred to $CHCl_3$ and CD_3OD at 7.26 and 3.34 for ^{1}H-NMR and at 77.0 and 49.0 ppm for ^{13}C-NMR respectively). HR-MS spectra were acquired by a Q-Exactive Hybrid Quadrupole-Orbitrap mass spectrometer (Thermo Scientific). TLC plates (Kieselgel 60 F254) and silica gel powder (Kieselgel 60, 0.063–0.200 mm) were from Merck.

All the reagents were purchased from Sigma-Aldrich and used without any further purification.

PARA-Naph-I1: hydantoinic building block (150 mg, 0.587 mmol) was dissolved in anhydrous DMF (6.0 mL); potassium carbonate (121 mg, 0.876 mmol) and TBAB (14 mg) were added; the mixture was heated at 50 °C under argon atmosphere with molecular sieves and α-bromo-1-acetonaphthone (176 mg, 0.416 mmol) was added after 15-30 min; after 2 h the reaction was evaporated and purified by silica gel chromatography using a gradient of chloroform and methanol to give compound **PARA-Naph-I1** (58 mg, 0.137 mmol, 33%); ^{1}H-NMR (CD_3OD): δ 8.89 (1H, bs, NH), 8.67 (1H, d, *J*= 8.37 Hz), 8.04 (1H, d, *J*= 8.2 Hz), 7.99 (1H, d, *J*= 7.27 Hz), 7.88 (1H, d, *J*= 7.95), 7.60-7.50 (2H, m, overlapped), 5.91 (1H, t, *J*= 8.23 Hz) 5.06 (2H, s), 3.22 (2H, m), 2.44 (2H, m) 1.44 (9H, s, Boc methyls); ^{13}C NMR (CD_3OD): δ 194.4 (C), 162.4 (C), 156.2 (C, Boc), 153.8 (C), 132.7 (CH), 127.6 (CH), 127.1 (CH) 124.9 (CH), 109.9 (CH), 80.2 (C, Boc), 45.1 (CH_2), 38.7 (CH_2), 26.8 (CH_2), 29.4, 29.0, 28.6 (CH_3, Boc methyls); HRMS (ESI) *m/z* 423.1798 $[M+Na]^+$ (calcd for $C_{23}H_{25}N_3O_5$, 423.1794).

PARA-Naph-I2: **PARA-Naph-I1** (58 mg, 0.137 mmol) was dissolved in ethanol (4 mL) and sodium borohydride (6 mg, 0.156 mmol) was added; the mixture was stirred for 2 h at room temperature and after addition of some drops of water was partitioned between water (20 mL) and ethylacetate (20 mL); the organic phase was evaporated to give **PARA-Naph-I2** (39 mg, 0.091 mmol, 66%); ^{1}H-NMR ($CDCl_3$): δ 8.25 (1H,m), 8.06 (1H, m), 7.88 – 7.70 (2H, m, overlapped), 7.58-7.32 (3H, m, overlapped), 5.86 (1H, m, overlapped) 5.79 (1H, m, overlapped, epimer,), 5.62 (1H, m, overlapped, epimer), 3.98 – 3.64 (4H, m, overlapped) 1.44 (9H, s, Boc methyls); ^{13}C NMR (CD_3OD): δ 170.7 (C), 164.7 (C), 155.3 (C, Boc), 127.7 (CH), 127.0 (CH) 124.7 (CH), 122.1 (CH), 110.1 (CH), 80.1 (C, Boc), 70.3 (CH, epimer), 68.2 (CH, epimer) 59.1 (CH_2), 47.6 (CH_2), 44. (CH_2), 27.7 (CH3, Boc methyls); HRMS (ESI) *m/z* 425.1948 $[M+Na]^+$ (calcd for $C_{23}H_{27}N_3O_5$, 425.1951).

PARA-Naph-I3: Compound **PARA-Naph-I2** (39 mg, 0.091 mmol) was dissolved in toluene (5 mL) with monohydrated p-toluensulfonic acid (70 mg, 0.37 mmol); the mixture was heated at 110 °C for 1

h, evaporated and partitioned between a saturated sodium bicarbonate water solution (100 mL) and chloroform (100 mL); chloroform was dried with sodium sulfate and purified further with silica gel chromatography using a gradient of chloroform and methanol to give **PARA-Naph-I3** (6 mg, 0.02 mmol, 22%); ^{1}H-NMR ($CDCl_3$): δ 8.33 (1H, d, *J* = 14.8 Hz), 8.14 (1H, d, *J* = 8.6 Hz), 7.90 (1H, d, *J* = 6.6 Hz), 7.90 (1H, d, *J* = 8.3 Hz), 7.83 (1H, d, *J* = 7.0 Hz), 7.76 (1H, d, *J* = 7.9 Hz), 7.65 – 7.41 (3H, m), 7.18 (1H, d, *J* = 14.5 Hz), 5.79 (1H, bt, *J* = 6.8 Hz), 2.87 (2H, m), 2.44 (2H, bq, *J* = 6.1 Hz); HRMS (ESI) *m/z* 308.1325 $[M+H]^+$ (calcd for $C_{18}H_{17}N_3O_2$, 307.1321).

PARA-Naph: Compound **PARA-Naph-I3** (8.6 mg, 0.02 mmol) was dissolved in anhydrous DMF (1.0 mL) with DIPEA (6 µL, 0.03 mmol) and 3,5-dimethyl-1-pyrazolylformaminidium nitrate (6 mg, 0.03 mmol); the mixture was stirred overnight at room temperature under argon atmosphere, evaporated, fractioned by silica gel chromatography using a gradient of chloroform and methanol and further purified by HPLC RP-phase (H_2O-TFA 0.1%/MeOH, from 60/40 to 50/50 in 20 minutes, RP-amide analytical column, flow rate 1 mL/min) to give PARA-Naph (3 mg, 0.008 mmol, 40%); ^{1}H-NMR (CD_3OD): δ 8.34 (1H, d, *J* = 14.2 Hz), 8.13 (1H, d, *J* = 8.5 Hz), 7.92 (1H, d, *J* = 6.6 Hz), 7.86 (1H, d, *J* = 8.3 Hz), 7.68 (1H, d, *J* = 7.0 Hz), 7.61 – 7.44 (3H, m), 7.22 (1H, d, *J* = 14.6 Hz), 5.89 (1H, bt, *J* = 7.8 Hz), 3.42 (2H, bt, *J* = 6.8 Hz), 2.60 (2H, bq, *J* = 7.0); ^{13}C NMR (CD_3OD): δ 162.5 (C), 157.2 (C=NH), 153.8 (C), 133.7 (C), 133.5 (C), 133.3 (C), 129.4 (CH), 128.9 (CH), 126.7 (CH), 124.5 (CH), 124.0 (CH), 119.9 (CH), 118.3 (CH), 110.1 (CH), 40.9 (CH2), 27.3 (CH2); HRMS (ESI) *m/z* 350.3277 $[M+H]^+$ (calcd for $C_{19}H_{19}N_5O_2$, 349.1539).

4.3. Biological assays

4.3.1. Cell cultures

GH4C1 rat pituitary adenoma cells were cultured in 50:50 DMEM:F12 medium containing penicillin/streptomycin and supplemented with L-glutamine and 10% of fetal bovine serum (FBS) and maintained in 5% CO2 in humidify air at 37°C [24].

4.3.2 Generation of CXCR4 knockout GH4 cells with CRISPR-Cas9

The CRISPR-Cas9 and green fluorescent protein (GFP) fusion protein expression vector U6RNA-Cas9-2A-GFP expressing gRNA targeting CXCR4 was purchased from Sigma-Aldrich. GH4C1 cells were plated in a 6-well plate in complete growth medium to achieve about 80% confluence on the day of transfection. Cells were transfected with Lipofectamine™ 3000 Transfection Reagent (ThermoFisher Scientific) according to the manufacturer's guidelines. The co-expression of Cas9 and GFP from the same mRNA allowed the possibility of tracking of transfection efficiency and enriching

cultures with CXCR4-knockout cells by fluorescence activated cell sorting (FACS) 24 h post-transfection. Cells were collected, diluted and seeded individually into 96-well plates, for isolating single colonies. Each colony was harvested and transferred to a 24-well plate. The cells were allowed to proliferate until checked for CXCR4 expression by RT-PCR and Western blot, and used for functional assays. Due to the lower residual expression of CXCR4 GH4C1 A11 clone was selected for the experiments.

4.3.3 Proliferation and viability assays

4.3.3.1 Cell proliferation assay CyQUANT®

DNA synthesis, as index of cell proliferation, was determined by fluorescence kit CyQUANT® (Life Technologies, USA). After treatments, GH4C1 and GH4A11 cells were incubated with CyQUANT® for 1 hr, as reported [34] The dye-DNA complexes were read using a microplate fluorescence reader (Tecan® Infinite 200 Pro, Switzerland) ex/em 485/530 nm.

4.3.3.2 Cell proliferation ELISA BrdU kit (Roche).

Modulation of GH4C1 cell proliferation induced by CXCL12 was evaluated by measuring 5-bromo-2'-deoxyuridine (BrdU) incorporation in newly synthesized cellular DNA [35]. Briefly, GH4C1 cells were seeded into 48 cluster plates at the density of 2.5x104 cells/well and treated for with CXCL12 (25 nM) in the absence or presence of tested compounds. After 20 hours, 10 µmol/l of BrdU was added to cell cultures and further incubated for 4 hours at 37 °C. subsequently cells were fixed and incubated with peroxidase-conjugated anti-BrdU antibodies. The amount of immunocomplexes was detected by adding peroxidase substrate tetramethyl benzidine. Reaction was stopped with 1M H2SO4. Absorbance was measured spectrophotometrically at 450 nm using microplate reader BioTek ELx800 (Winooski VT, USA).

4.3.4 MTT reduction assay

Mitochondrial function, as index of cell viability, was evaluated by measuring intracellular reduction of 3-(4,5-Dimethyl-2-thiazolyl)-2,5-diphenyl-2H-tetrazolium bromide (MTT, Sigma-Aldrich) to water insoluble purple formazan by mitochondrial dehydrogenase [36]. Briefly, 0.25 mg/ml MTT was added to culture medium and incubated at 37°C for 3 hrs; medium was then removed, and formazan crystals were dissolved in dimethylsulfoxide. Absorbance was measured spectrophotometrically at 570 nm using microplate reader BioTek ELx800 (Winooski VT, USA).

4.3.5 Migration assay

Modulation of CXCL12-induced chemoattraction of GH4C1 and GH4A11 cells was assayed measuring cell migration through microporous membranes [37]. Cells were plated into 6 well clusters at a density of 30x104 cells/well, serum deprived for 48 hours and treated with the different compounds at the

concentration of 1 μM. After 12 hours of treatment cells were stained with fluorescent dye Vybrant™ CFDA SE (ThermoFisher) 10μM for 15 min at 37 °C, gently harvested in serum free medium and plated in the upper chambers of FluoroBlok™ HTS 96 multiwell (8 μm pore, Corning) at the concentration of 1.5x104 per chamber. CXCL12 (25 nM) was added in the lower compartment and migration was evaluated after six hours by counting the number of the cells that have migrated in the lower chambers with confocal microscope (BioRad MRC 1024 ES) (3 microscopic fields for each condition). The medium in upper and lower chamber was devoid of fetal bovine serum throughout the experiment to avoid unspecific chemoattraction.

4.3.6 Immunoblotting

Cells were plated in 60 mm petri dishes (2 × 105/ dish), serum deprived for 48 hours and treated with SDF-1α in the absence or the presence of PARA compounds. After 15 min of treatment cells were lysed in Tris-Hcl 20 mM pH 8 NACl 137 mM, EDTA 2 mm, glycerol 10%, NP-40 1%, phenylmethylsulfonyl fluoride 1 mM and cOmplete Mini protease inhibitor cocktail (Roche)[38]. After centrifugation (10 min, 500 x g) to remove nuclei, concentration of protein in cytoplasmic fractions was assessed by Bradford assay. 30 μg of proteins from each sample were boiled in Laemmli buffer and size-fractionated by 12% SDS-PAGE. Resolved proteins were electroblotted onto 0.2 μm polyvinylidene difluoride membrane (Bio-Rad Laboratories) and probed with primary antibodies. Immunoreactive bands were visualized adding HRP-labeled secondary antibodies followed by Clarity TM Western ECL (Bio-Rad Laboratories) and quantified using ChemiDoc imaging system, equipped with Image lab 4.0.1 software (Bio-Rad Laboratories). Quantification of the signal was performed by densitometry and measured as ratios of housekeeping (α-tubulin or β-actin) used to normalize protein content.

4.3.7 Antibodies

P42/44 ERK1/2 and phospho-p44/42 (ERK1/2) rabbit polyclonal antibodies (Cell signaling). CXCR4, monoclonal mouse antibody (Abcam). α-tubulin and β-actin, monoclonal mouse antibodies (Sigma Aldrich). HRP-conjugated anti-rabbit IgG goat antiserum (Bio-Rad Laboratories).

4.3.8 Statistical analysis

All data are presented as mean ± SEM of at least three experiments performed in triplicate. Statistical significance was established at p-value < 0.05. Prism version 5.02 (GraphPad, San Diego, CA) software was used to analyze the results.

Bibliography

[1] A. Zlotnik, O. Yoshie, The Chemokine Superfamily Revisited, Immunity. 36 (2012) 705–716. doi:10.1016/j.immuni.2012.05.008.

[2] C.A. Didigu, R.W. Doms, Novel Approaches to Inhibit HIV Entry, Viruses. 4 (2012) 309–324. doi:10.3390/v4020309.

[3] P.A. Hernandez, R.J. Gorlin, J.N. Lukens, S. Taniuchi, J. Bohinjec, F. Francois, M.E. Klotman, G.A. Diaz, Mutations in the chemokine receptor gene CXCR4 are associated with WHIM syndrome, a combined immunodeficiency disease, Nat. Genet. 34 (2003) 70–74. doi:10.1038/ng1149.

[4] J.S. Song, C.M. Kang, H.H. Kang, H.K. Yoon, Y.K. Kim, K.H. Kim, H.S. Moon, S.H. Park, Inhibitory effect of CXC chemokine receptor 4 antagonist AMD3100 on bleomycin induced murine pulmonary fibrosis, Exp. Mol. Med. 42 (2010) 465. doi:10.3858/emm.2010.42.6.048.

[5] A. Wang, A.-M. Fairhurst, K. Tus, S. Subramanian, Y. Liu, F. Lin, P. Igarashi, X.J. Zhou, F. Batteux, D. Wong, E.K. Wakeland, C. Mohan, CXCR4/CXCL12 Hyperexpression Plays a Pivotal Role in the Pathogenesis of Lupus, J. Immunol. 182 (2009) 4448–4458. doi:10.4049/jimmunol.0801920.

[6] A. Bajetto, F. Barbieri, A. Pattarozzi, A. Dorcaratto, C. Porcile, J.L. Ravetti, G. Zona, R. Spaziante, G. Schettini, T. Florio, CXCR4 and SDF1 expression in human meningiomas: a proliferative role in tumoral meningothelial cells in vitro., Neuro. Oncol. 9 (2007) 3–11. http://www.hubmed.org/display.cgi?uids=17108064.

[7] B.A. Teicher, S.P. Fricker, CXCL12 (SDF-1)/CXCR4 pathway in cancer., Clin. Cancer Res. 16 (2010) 2927–2931. http://www.hubmed.org/display.cgi?uids=20484021.

[8] X. Sun, G. Cheng, M. Hao, J. Zheng, X. Zhou, J. Zhang, R.S. Taichman, K.J. Pienta, J. Wang, CXCL12 / CXCR4 / CXCR7 chemokine axis and cancer progression., Cancer Metastasis Rev. 29 (2010) 709–722. http://www.hubmed.org/display.cgi?uids=20839032.

[9] H. Maganti, A. Visram, R. Shorr, J. Fulcher, M. Sabloff, D.S. Allan, Plerixafor in combination with chemotherapy and/or hematopoietic cell transplantation to treat acute leukemia: A systematic review and metanalysis of preclinical and clinical studies, Leuk. Res. 97 (2020) 106442. doi:10.1016/j.leukres.2020.106442.

[10] S. Milanesi, M. Locati, E.M. Borroni, Aberrant CXCR4 Signaling at Crossroad of WHIM Syndrome and Waldenstrom's Macroglobulinemia, Int. J. Mol. Sci. 21 (2020) 5696. doi:10.3390/ijms21165696.

[11] R.J. Miller, G. Banisadr, B.J. Bhattacharyya, CXCR4 signaling in the regulation of stem cell

migration and development, J. Neuroimmunol. 198 (2008) 31–38. doi:10.1016/j.jneuroim.2008.04.008.

[12] E. De Clercq, The AMD3100 story: the path to the discovery of a stem cell mobilizer (Mozobil), Biochem. Pharmacol. 77 (2009) 1655–1664. doi:10.1016/j.bcp.2008.12.014.

[13] N.D. Stone, S.B. Dunaway, C. Flexner, C. Tierney, G.B. Calandra, S. Becker, Y.-J. Cao, I.P. Wiggins, J. Conley, R.T. MacFarland, J.-G. Park, C. Lalama, S. Snyder, B. Kallungal, K.L. Klingman, C.W. Hendrix, Multiple-Dose Escalation Study of the Safety, Pharmacokinetics, and Biologic Activity of Oral AMD070, a Selective CXCR4 Receptor Inhibitor, in Human Subjects, Antimicrob. Agents Chemother. 51 (2007) 2351–2358. doi:10.1128/AAC.00013-07.

[14] S. Jenkinson, M. Thomson, D. McCoy, M. Edelstein, S. Danehower, W. Lawrence, P. Wheelan, A. Spaltenstein, K. Gudmundsson, Blockade of X4-Tropic HIV-1 Cellular Entry by GSK812397, a Potent Noncompetitive CXCR4 Receptor Antagonist, Antimicrob. Agents Chemother. 54 (2010) 817–824. doi:10.1128/AAC.01293-09.

[15] W.-T. Hsu, H.-Y. Jui, Y.-H. Huang, M.-Y.M. Su, Y.-W. Wu, W.-Y.I. Tseng, M.-C. Hsu, B.-L. Chiang, K.K. Wu, C.-M. Lee, CXCR4 Antagonist TG-0054 Mobilizes Mesenchymal Stem Cells, Attenuates Inflammation, and Preserves Cardiac Systolic Function in a Porcine Model of Myocardial Infarction, Cell Transplant. 24 (2015) 1313–1328. doi:10.3727/096368914X681739.

[16] T. Murakami, S. Kumakura, T. Yamazaki, R. Tanaka, M. Hamatake, K. Okuma, W. Huang, J. Toma, J. Komano, M. Yanaka, Y. Tanaka, N. Yamamoto, The Novel CXCR4 Antagonist KRH-3955 Is an Orally Bioavailable and Extremely Potent Inhibitor of Human Immunodeficiency Virus Type 1 Infection: Comparative Studies with AMD3100, Antimicrob. Agents Chemother. 53 (2009) 2940–2948. doi:10.1128/AAC.01727-08.

[17] X. Fang, Q. Meng, H. Zhang, B. Liang, S. Zhu, J. Wang, C. Zhang, L.S. Huang, X. Zhang, R.T. Schooley, J. An, Y. Xu, Z. Huang, Design, synthesis, and biological characterization of a new class of symmetrical polyamine-based small molecule CXCR4 antagonists, Eur. J. Med. Chem. 200 (2020) 112410. doi:10.1016/j.ejmech.2020.112410.

[18] R.M. Vitale, M. Gatti, M. Carbone, F. Barbieri, V. Felicità, M. Gavagnin, T. Florio, P. Amodeo, Minimalist Hybrid Ligand/Receptor-Based Pharmacophore Model for CXCR4 Applied to a Small-Library of Marine Natural Products Led to the Identification of Phidianidine A as a New CXCR4 Ligand Exhibiting Antagonist Activity, ACS Chem. Biol. 8 (2013) 2762–2770. doi:10.1021/cb400521b.

[19] N. Cachet, G. Genta-Jouve, E.L. Regalado, R. Mokrini, P. Amade, G. Culioli, O.P. Thomas, Parazoanthines A−E, Hydantoin Alkaloids from the Mediterranean Sea Anemone Parazoanthus

axinellae, J. Nat. Prod. 72 (2009) 1612–1615. doi:10.1021/np900437y.

[20] C. Audoin, V. Cocandeau, O. Thomas, A. Bruschini, S. Holderith, G. Genta-Jouve, Metabolome Consistency: Additional Parazoanthines from the Mediterranean Zoanthid Parazoanthus Axinellae, Metabolites. 4 (2014) 421–432. doi:10.3390/metabo4020421.

[21] J. Wefer, T. Lindel, Total Synthesis of the Marine Natural Product Parazoanthine F by Copper-Mediated C-N Coupling, European J. Org. Chem. 2015 (2015) 6370–6381. doi:10.1002/ejoc.201500823.

[22] E. Manzo, D. Pagano, G. Nuzzo, M. Gavagnin, M.L. Ciavatta, First synthesis of parazoanthine-A and its O-Me derivative, Tetrahedron Lett. 53 (2012) 7083–7084. doi:10.1016/j.tetlet.2012.10.066.

[23] F. Tinto, D. Pagano, E. Manzo, Synthesis of parazoanthine B and analogs, Tetrahedron. 71 (2015) 4379–4384. doi:10.1016/j.tet.2015.04.040.

[24] T. Florio, S. Casagrande, F. Diana, A. Bajetto, C. Porcile, G. Zona, S. Thellung, S. Arena, A. Pattarozzi, A. Corsaro, R. Spaziante, M. Robello, G. Schettini, Chemokine Stromal Cell-Derived Factor 1α Induces Proliferation and Growth Hormone Release in GH4C1 Rat Pituitary Adenoma Cell Line through Multiple Intracellular Signals, Mol. Pharmacol. 69 (2006) 539–546. doi:10.1124/mol.105.015255.

[25] F. Barbieri, A. Bajetto, R. Stumm, A. Pattarozzi, C. Porcile, G. Zona, A. Dorcaratto, J.-L. Ravetti, F. Minuto, R. Spaziante, G. Schettini, D. Ferone, T. Florio, Overexpression of Stromal Cell-Derived Factor 1 and Its Receptor CXCR4 Induces Autocrine/Paracrine Cell Proliferation in Human Pituitary Adenomas, Clin. Cancer Res. 14 (2008) 5022–5032. doi:10.1158/1078-0432.CCR-07-4717.

[26] R. Würth, F. Barbieri, A. Pattarozzi, G. Gaudenzi, F. Gatto, P. Fiaschi, J.-L. Ravetti, G. Zona, A. Daga, L. Persani, D. Ferone, G. Vitale, T. Florio, Phenotypical and Pharmacological Characterization of Stem-Like Cells in Human Pituitary Adenomas, Mol. Neurobiol. 54 (2017) 4879–4895. doi:10.1007/s12035-016-0025-x.

[27] R. Würth, A. Bajetto, J.K. Harrison, F. Barbieri, T. Florio, CXCL12 modulation of CXCR4 and CXCR7 activity in human glioblastoma stem-like cells and regulation of the tumor microenvironment, Front. Cell. Neurosci. 8 (2014). doi:10.3389/fncel.2014.00144.

[28] B. Hitchinson, J.M. Eby, X. Gao, F. Guite-Vinet, J.J. Ziarek, H. Abdelkarim, Y. Lee, Y. Okamoto, S. Shikano, M. Majetschak, N. Heveker, B.F. Volkman, N.I. Tarasova, V. Gaponenko, Biased antagonism of CXCR4 avoids antagonist tolerance, Sci. Signal. 11 (2018) eaat2214. doi:10.1126/scisignal.aat2214.

[29] G.M. Morris, R. Huey, W. Lindstrom, M.F. Sanner, R.K. Belew, D.S. Goodsell, A.J. Olson, AutoDock4 and AutoDockTools4: Automated docking with selective receptor flexibility, J. Comput. Chem. 30 (2009) 2785–2791. doi:10.1002/jcc.21256.

[30] N. Eswar, B. Webb, M.A. Marti-Renom, M.S. Madhusudhan, D. Eramian, M.-Y. Shen, U. Pieper, A. Sali, Comparative Protein Structure Modeling Using Modeller, in: Curr. Protoc. Bioinforma., John Wiley & Sons, Inc., Hoboken, NJ, USA, 2006: pp. 5.6.1-5.6.30. doi:10.1002/0471250953.bi0506s15.

[31] H.G. D.A. Case, R.M. Betz, D.S. Cerutti, T.E. Cheatham, III, T.A. Darden, R.E. Duke, T.J. Giese, C. A.W. Goetz, N. Homeyer, S. Izadi, P. Janowski, J. Kaus, A. Kovalenko, T.S. Lee, S. LeGrand, P. Li, I. Lin, T. Luchko, R. Luo, B. Madej, D. Mermelstein, K.M. Merz, G. Monard, H. Nguyen, H.T. Nguyen, J.S. Omelyan, A. Onufriev, D.R. Roe, A. Roitberg, C. Sagui, C.L. Simmerling, W.M. Botello-Smith, L.X. and P.A.K. R.C. Walker, J. Wang, R.M. Wolf, X. Wu, AMBER 2016, (2016).

[32] T. Fox, P.A. Kollman, Application of the RESP Methodology in the Parametrization of Organic Solvents, J. Phys. Chem. B. 102 (1998) 8070–8079. doi:10.1021/jp9717655.

[33] M.S. Gordon, M.W. Schmidt, Advances in electronic structure theory, in: C.E. Dykstra, G. Frenking, K.S. Kim, G.E. Scuseria (Eds.), Theory Appl. Comput. Chem., Elsevier, Amsterdam, 2005: pp. 1167–1189. doi:10.1016/B978-044451719-7/50084-6.

[34] V. Villa, S. Thellung, A. Corsaro, F. Novelli, B. Tasso, L. Colucci-D'Amato, E. Gatta, M. Tonelli, T. Florio, Celecoxib Inhibits Prion Protein 90-231-Mediated Pro-inflammatory Responses in Microglial Cells, Mol. Neurobiol. 53 (2016) 57–72. doi:10.1007/s12035-014-8982-4.

[35] A. Pattarozzi, E. Carra, R.E. Favoni, R. Würth, D. Marubbi, R.A. Filiberti, L. Mutti, T. Florio, F. Barbieri, A. Daga, The inhibition of FGF receptor 1 activity mediates sorafenib antiproliferative effects in human malignant pleural mesothelioma tumor-initiating cells, Stem Cell Res. Ther. 8 (2017) 119. doi:10.1186/s13287-017-0573-7.

[36] F. Barbieri, R. Würth, A. Pattarozzi, I. Verduci, C. Mazzola, M.G. Cattaneo, M. Tonelli, A. Solari, A. Bajetto, A. Daga, L.M. Vicentini, M. Mazzanti, T. Florio, Inhibition of Chloride Intracellular Channel 1 (CLIC1) as Biguanide Class-Effect to Impair Human Glioblastoma Stem Cell Viability, Front. Pharmacol. 9 (2018). doi:10.3389/fphar.2018.00899.

[37] M. Gatti, A. Solari, A. Pattarozzi, C. Campanella, S. Thellung, L. Maniscalco, R. De Maria, R. Würth, A. Corsaro, A. Bajetto, A. Ratto, A. Ferrari, A. Daga, F. Barbieri, T. Florio, In vitro and in vivo characterization of stem-like cells from canine osteosarcoma and assessment of drug

sensitivity, Exp. Cell Res. 363 (2018) 48–64. doi:10.1016/j.yexcr.2018.01.002.

[38] A. Bajetto, A. Pattarozzi, A. Corsaro, F. Barbieri, A. Daga, A. Bosio, M. Gatti, V. Pisaturo, R. Sirito, T. Florio, Different Effects of Human Umbilical Cord Mesenchymal Stem Cells on Glioblastoma Stem Cells by Direct Cell Interaction or Via Released Soluble Factors, Front. Cell. Neurosci. 11 (2017). doi:10.3389/fncel.2017.00312.